Pressure-induced structural transitions and metallization in Ag_2Te

Zhao Zhao,[1] Shibing Wang,[2,3] Haijun Zhang,[1] and Wendy L. Mao[2,4]
[1]*Department of Physics, Stanford University, Stanford, California 94305, USA*
[2]*Department of Geological and Environmental Sciences, Stanford University, Stanford, California 94305, USA*
[3]*Stanford Synchrotron Radiation Light Source, SLAC National Accelerator Laboratory, Menlo Park, California 94025, USA*
[4]*Photon Science, SLAC National Accelerator Laboratory, Menlo Park, California 94025, USA*
(Received 21 December 2012; revised manuscript received 6 May 2013; published 31 July 2013)

High-pressure *in situ* synchrotron x-ray diffraction experiments were performed on Ag_2Te up to 42.6 GPa at room temperature, and four phases were identified. Phase I (β–Ag_2Te) transformed into isostructural phase II at 2.4 GPa, and phase III and phase IV emerged at 2.8 and 12.8 GPa, respectively. Combined with first-principles calculations, we solved the phase II and phase III crystal structures and determined the compressional behavior of phase III. Electronic band structure calculations show that the insulating phase I with a narrow band gap first transforms into the semimetallic phase II with the perseverance of topologically nontrivial nature and then to the bulk metallic phase III. Density of states calculations indicate the contrasting transport behavior for $Ag_{2-\delta}Te$ and $Ag_{2+\delta}Te$ under compression. Our results highlight pressure's dramatic role in tuning Ag_2Te's electronic band structure and its novel electrical and magnetotransport behaviors.

DOI: 10.1103/PhysRevB.88.024120 PACS number(s): 62.50.−p, 71.30.+h

I. INTRODUCTION

Topological insulator is an interesting field in condensed matter recently, where many of topological insulators unusual physical properties originate from the topological surface metallic states.[1–4] For previous well-studied three-dimensional (3D) topological insulators such as Bi_2Te_3 and Bi_2Se_3, the surface states form a highly isotropic Dirac cone, as determined by the high-symmetry hexagonal crystal lattice.[5–9] Yet based on recent calculations, ambient-condition silver telluride (Ag_2Te) is a potential 3D topological insulator with a highly anisotropic Dirac cone due to its low monoclinic crystal symmetry.[10] Experimentally, the existence of metallic surface states is supported by evidence of the pronounced Aharanov-Bohm oscillation, which is observed in single crystalline β–Ag_2Te nanowires and nanoribbons,[11,12] similar to the case of nanosized Bi_2Se_3 and Bi_2Te_3.[13,14] For a topological insulator with a highly anisotropic Dirac, novel physics such as spin conduction is expected.[15,16]

Unusually large linear magnetoresistance (LMR) was observed in Ag_2Te in magnetic fields up to 55 kOe, from 5 K to room temperature,[17] making it a promising material for industrial applications, such as magnetic field sensors fabrication.[18] To explain the novel LMR, classical and quantum explanations had been proposed earlier. The classical solution emphasized the inhomogeneous distribution of Ag ions and large spatial fluctuations in the conductivity of a two-dimensional system where the gap goes to zero.[19–21] However, the quantum solution assumed a gapless spectrum with linear momentum dependence between the valence and the conduction bands and strong disorder in the Ag_2Te system.[22,23] The most recent prediction that Ag_2Te is a 3D topological insulator can also explain the LMR properly, where the linear behavior is induced by the surface states.[10]

Pressure is a powerful tool to induce dramatic changes in the interatomic distances and atomic arrangements and thus to tune materials' properties. A previous electrical and magnetotransport study on Ag_2Te showed that pressure has significant effects on the electrical resistivity and magnetoresistive (MR) behaviors and can modify the electronic band structure.[24] Despite these interesting high-pressure phenomena, only few high-pressure structural studies on Ag_2Te have been reported, and the space group of the high-pressure phases has not been determined.[25] To solve the high-pressure Ag_2Te structures and explore their related electronic properties, especially the robustness of the surface states, we performed *in situ* synchrotron angle-dispersive powder x-ray diffraction (XRD) experiments and first-principles calculations on Ag_2Te. In this paper, we report on the new structural models of Ag_2Te at high pressure and their calculated electronic band structures.

At room temperature and ambient pressure, bulk Ag_2Te is a narrow band gap insulator with a monoclinic crystal structure (space group $P2_1/c$, $Z = 4$) called β–Ag_2Te. Its strongly distorted antifluorite structure has a triple-layered Te (Ag)–Ag–Te (Ag) stacking structure, where the Te atoms occupy a distorted face-centered cubic (FCC) lattice with Ag atoms inserted in the interstitials[11,26] [Fig. 1(b)]. When heated above 417 K, it transforms into superionic α–Ag_2Te, which has a FCC structure (space group $Fm\bar{3}m$, $Z = 4$).[27,28]

II. EXPERIMENTS AND CALCULATION METHODS

In our experiments, high-purity powder Ag_2Te (Product No. 400645, Lot No. MKBG0692V) was purchased from the supplier Sigma-Aldrich. The purity and homogeneity are checked by x-ray photoemission spectrum and electron microprobe analysis at Stanford Nanocharacterization Laboratory, shown in the Supplemental Material.[29] Symmetric diamond anvil cells with a 300-μm culet size were used. Tungsten thin foils were used as the gasket, and a 120-μm-diameter sample chamber was drilled in the center. Ruby spheres were used for determining pressure. In two separate experiments, silicone oil was used as the pressure medium to study the low-pressure region up to 4.7 GPa ($\lambda = 0.6199$ Å) and neon gas was used as the pressure medium to maintain hydrostatic condition to reach 42.6 GPa ($\lambda = 0.37379$ Å). Angle-dispersive XRD experiments were performed at beamlines 16-IDB and

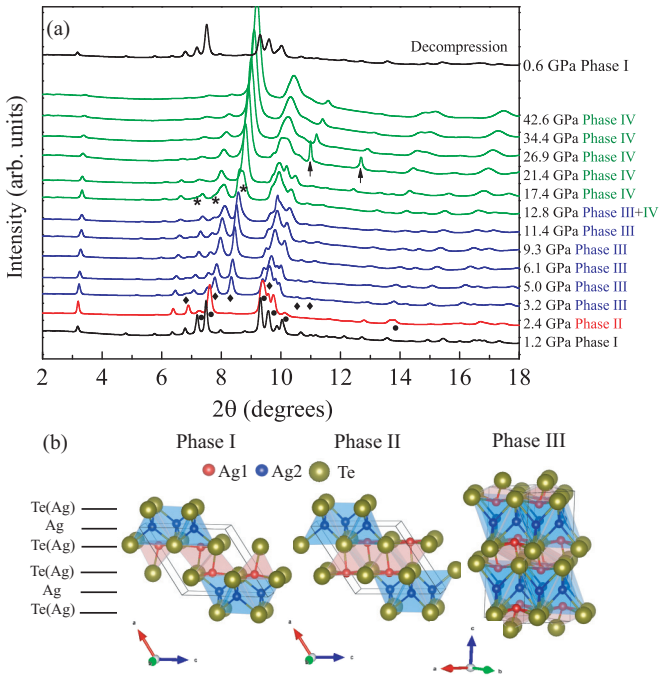

FIG. 1. (Color online) (a) Representative XRD patterns for Ag_2Te under pressure up to 42.6 GPa ($\lambda = 0.373\,79$ Å). Either new peaks or peaks with different intensity are marked by circles, diamonds, and asterisks for phases II, III, and IV, correspondently. Arrows indicate diffraction peaks from the Ne pressure medium. (b) Schematic view of Ag_2Te phase I, II, and III structures.

16-BMD of the Advanced Photon Source (APS), Argonne National Laboratory, and 12.2.2 of the Advanced Light Source (ALS), Lawrence Berkeley National Laboratory. Jade was used for space group indexing,[30] and Rietveld refinement was performed using the General Structure Analysis System (GSAS) and graphical user interface EXPGUI package.[31]

For calculations, the Vienna *Ab initio* Simulation Package[32,33] was employed for the crystal structure relaxations within the framework of Perdew-Burke-Ernzerhof–type[34] generalized gradient approximation of density functional theory.[35] The projector-augmented wave[36] pseudopotential was used for all calculations.

III. RESULTS AND DISCUSSION

Representative XRD patterns from the experiment using neon as pressure medium ($\lambda = 0.373\,79$ Å) are shown in Fig. 1(a); the second set of data ($\lambda = 0.6199$ Å) is shown in the Supplemental Material.[29] New peaks and those with significantly different intensity are marked to distinguish new phases. The lowest pressure diffraction measurement at 1.2 GPa confirms the ambient β–Ag_2Te (phase I) monoclinic structure.[26] The measurement taken at 2.4 GPa shows a different pattern and indicates the appearance of phase II. Phase III emerges at 2.8 GPa, and the transformation completes at 3.2 GPa. Phase III starts to transform into phase IV at 12.8 GPa and transforms at 17.2 GPa. Phase IV persists to the highest pressure measured. Under compression, the largest d spacing peak corresponds to the stacking distance of Te(Ag)–Ag–Te(Ag) triple-layered structure and shifts continuously to smaller d spacings up to 42.6 GPa. Decompression experiments show that all phase transitions are reversible: phase III appears at 11.1 GPa, phase II appears at 2.4 GPa, and phase I appears at 1.9 GPa.

Figure 1(b) shows the structures of phases I, II, and III. Phase I has a monoclinic structure with four Ag_2Te formula per unit cell and two different Ag sites.[26] We found that phase II is isostructural to phase I and phase III has an orthorhombic structure with space group *Cmca*, $Z = 8$. Representative Rietveld refinement results and profiles are presented in the Supplemental Material.[29] From phase I to phase II, the strong decrease in the intensity of peaks such as $(21\bar{1})$ and (111) (at $2\theta = 7.215°$ and $7.268°$) were observed without additional new peaks; thus, phase II is assigned to the same monoclinic space group of phase I. In previous literature,[25] the features (see Fig. S3(a) in the Supplemental Material),[29] which we identify as separate (112) and $(31\bar{2})$ peaks, were considered a single reflection. Our data clearly show that the symmetry of phase II has to be lower than the previously proposed tetragonal symmetry.[25] We also relaxed all atoms in the monoclinic phase II structure from the Rietveld refinement, and its band structure does not change, indicating that the structure we solved is stable electronically.

Phase III is assigned to an orthorhombic structure with the centrosymmetric space group *Cmca*. The inversion center is in the middle of two nearest triple Te (Ag)–Ag–Te (Ag) layers. The Rietveld refinement profile for the *Cmca* structure is shown in Fig. S3(b). The clear separation between diffraction peaks such as (022) and (202) indicates unequal a and b and thus refutes the early proposed tetragonal symmetry.[25] We also identified another highly similar structure with a noncentrosymmetric *Aba*2 space group that can give an equally good Rietveld fit. The two structures could be differentiated by that in the *Cmca* structure Ag1-Te3 and Ag1-Te5 have the same distances, while they are different in the *Aba2* structure. To determine which structure is energetically favorable, we used experimental lattices for these two structures at 5.0 and 11.4 GPa and relaxed the atomic positions at the two space groups by first-principles calculations. The results show that these two structures have a negligible difference in energy: at 5.0 and 11.4 GPa, the differences are within 5 meV per unit cell. Considering that *Aba*2 is a subgroup of *Cmca*, we assign phase III to the higher symmetry *Cmca* structure.

Two Ag sites, Ag1 and Ag2, exist for phases I, II, and III (inset of Fig. 2). From phase I to phase II (Fig. 2), the striking difference is the Ag1-Te2 distance dropped from ~3.6 to 3.4 Å, increasing the coordination number for Ag1 from four to five, as shown in Fig. 1(b). The coordination of Ag2 remains four in all three phases. Figure 3 presents the evolution of volume per Ag_2Te formula unit with increasing pressure, and the inset shows normalized lattice parameters for phase III. In phase III, the a direction lying in the layers stacking plane is slightly more compressible than it is in the b and c directions. The c axis is not the most compressible, which suggests strong interlayer bonding—totally different from other topological insulators such as Bi_2Te_3 and Bi_2Se_3 with Van der Waals layers.[37,38] For phase III of Ag_2Te, the in-plane compression anisotropy in the a and b directions shows increasing Ag-Te tetrahedral and

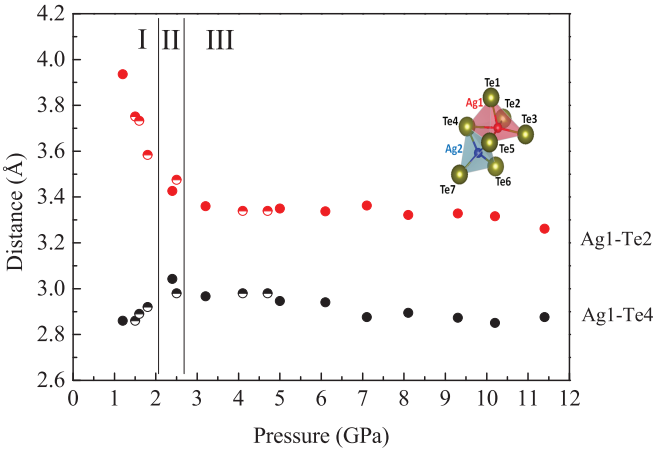

FIG. 2. (Color online) Selected Ag1 to nearby Te distance vs pressure. Filled and half-filled circles are from experiments with Ne and silicone oil, respectively, as the pressure medium. Errors given by the GSAS EXPGUI package are smaller than the marker sizes.

octahedral distortions that may come from increasing ionic interactions at high pressure.

In order to determine the electronic structure of different phases, we carried out first-principles calculations. The kinetic energy cutoff was fixed to 450 eV, and spin-orbit coupling interaction was included through the non-self-consistent calculation. Phase I is proposed as a topological insulator,[10] with topological surface states including an odd number of gapless Dirac cones inside the bulk band gap. Our band structure calculation for phase I agrees well with a previous study,[10] shown in Fig. 4(a). The red dots show the character of the Ag *s* orbital. The band inversion can be seen clearly near the Γ point. In the comparison shown in Fig. 4(b), phase II becomes a semimetal, as there are only a few states crossing the Fermi level, for instance, the valence band between Z and Γ raised

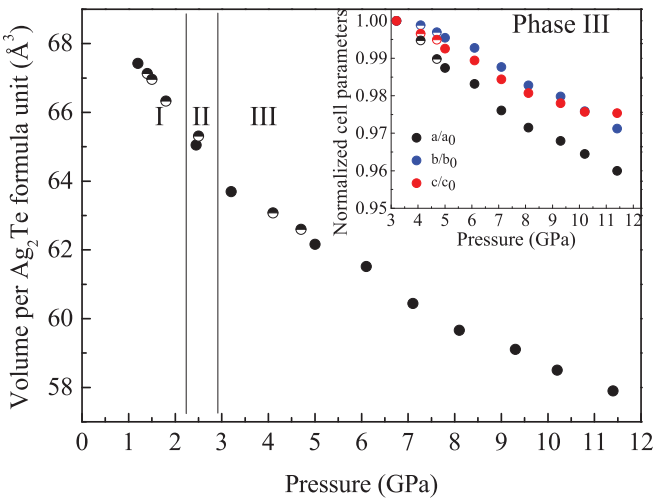

FIG. 3. (Color online) Volume per Ag_2Te formula unit vs pressure. The inset shows the normalized cell parameters a/a_0, b/b_0, and c/c_0. Filled and half-filled circles are from experiments with Ne and silicone oil, respectively, as the pressure medium. Errors given by the GSAS EXPGUI package are smaller than the marker sizes.

above Fermi level. The band inversion around the Γ point still exists, so its topologically nontrivial nature is maintained and the bulk metallic states may mix with the surface metallic states. The band structure of phase III is shown in Fig. 4(c). The large band overlap between the conduction and the valence bands clearly shows that phase III becomes a bulk metal; thus, it is unnecessary to define its topological nature.

Based on these electronic structures, the previous high-pressure magnetotransport results of Ag_2Te[24] can now be understood. For phases II and III, different MR responses are expected based on conventional band theory with a closed Fermi surface.[39] In phase II, the bulk metallic properties dominate the surface properties; thus, the MR will have more quadratic character. In phase III, the system becomes a bulk metal and thus results in a completely quadratic MR response. Previously reported low-temperature transport measurements on $Ag_{2-\delta}Te$ at 1.01, 1.35, and 1.71 GPa showed decreasing electrical resistivity and gradual weakening of LMR, and a clear quadratic MR response was observed at 1.71 GPa.[24] These results indicate comparatively large band structure evolution near the Fermi surface for $Ag_{2-\delta}Te$ under pressure, and 1.71 GPa should be close to the transition between the insulating phase I and the semimetallic phase II at 4.2 K.

Figure 4(d) shows the calculated density of states (DOS) of phases I, II, and III. Among them, phase III has the highest DOS. From -0.12 eV to below the Fermi level (of stoichiometric Ag_2Te), phase II has a lower DOS than that of phase I. Yet from above -0.12 to 0.2 eV the DOS of phase II is much greater than that of phase I. In the case of a minor amount of self-doping in $Ag_{2-\delta}Te$ and $Ag_{2+\delta}Te$, the crystal structure should be the same and the band structure features will be maintained, with a mere adjustment of the Fermi level. For silver-rich $Ag_{2+\delta}Te$ (*n* type), the Fermi level will shift to higher energy. The increase of the DOS will lead to decreased electrical resistivity with increasing pressure from the phase I to the phase II regime. For silver-deficient $Ag_{2-\delta}Te$ (*p* type), the situation is interesting: Depending on the doping ratio, the shifting Fermi level may drop into the low-energy (-0.12 to $\sim$0 eV) region or even lower-energy (less than -0.12 eV) region. In these two regions, different transport behavior is expected. We roughly estimated that the value of δ that can shift the Fermi level down 0.12 eV is 0.02. The earlier room-temperature transport measurements showed that phase II was less conductive than phase I and phase III was twice as conductive as phase I.[25] This may because they were measured on a $Ag_{2-\delta}Te$ ($\delta > 0.02$) sample where phase II has a smaller DOS than does phase I at that doping ratio. Phase III is the most conductive for its largest DOS near the Fermi level at all doping ratios.

The following techniques can provide useful information on the band gap of Ag_2Te. Angle-resolved photoemission spectroscopy study on high-quality stoichiometric Ag_2Te may reveal the existence of metallic surface states experimentally. High-pressure optical infrared study can show evidence for the metallization process. In addition, systematic high-pressure electronic and magnetotransport study on different δ samples of $Ag_{2+\delta}Te$ and $Ag_{2-\delta}Te$ samples may find more properties concerning the topological surface states' evolution under compression. Measurements on nanoribbons and nanowires

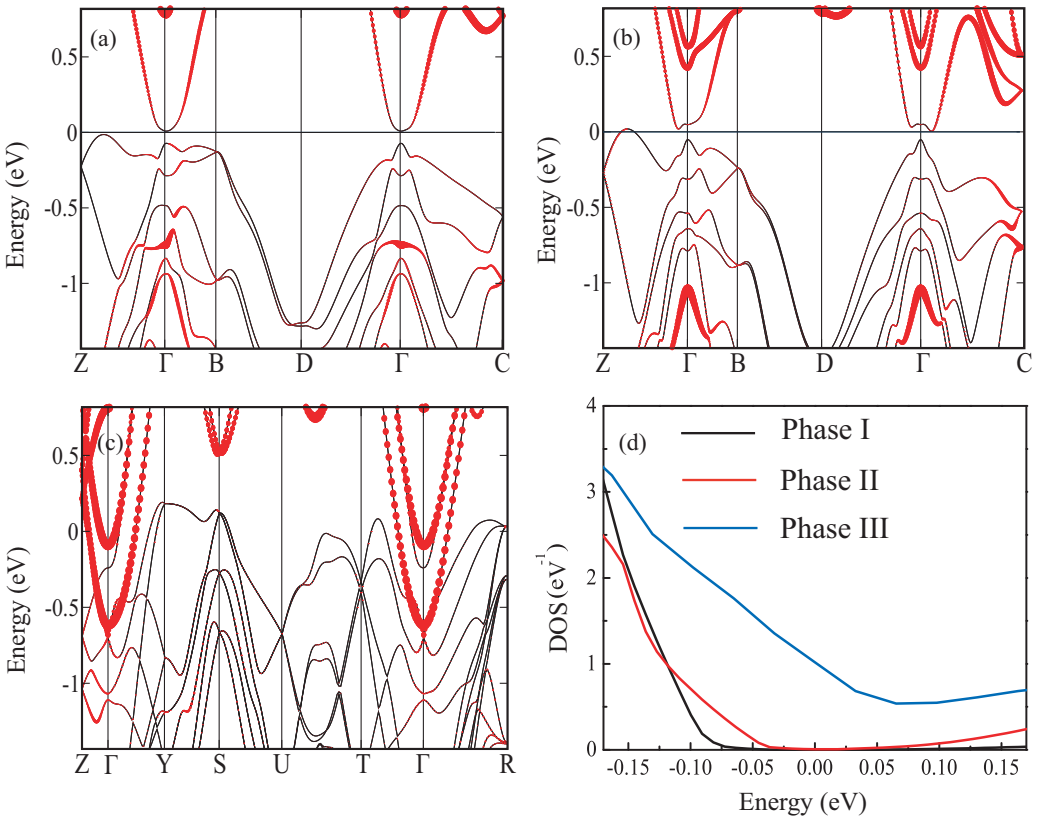

FIG. 4. (Color online) Calculated band structure of (a) phase I, (b) phase III, and (c) phase III. The red dots indicate the projection of the Ag *s* orbital; in (a) and (b), it goes down to occupied from unoccupied around Γ, which indicates the band inversion. In (d), Fermi level is shifted to 0 eV. These band structures present (a) phase I with a narrow band gap, (b) the semimetallic phase II, and (c) the metallic phase III. (d) Calculated DOS of phases I, II, and III.

would be equally interesting because of the potentially increased surface contributions to the bulk properties.

IV. CONCLUSIONS

The structure of Ag_2Te up to 42.6 GPa at room temperature was studied by *in situ* synchrotron angle-dispersive XRD and first-principles calculations. Three phases were identified at high pressure. Phase II is solved to be an isostructure to monoclinic phase I, and phase III has an orthorhombic structure. Pressure strongly modifies the electronic band structure of Ag_2Te: Phase II preserves the band inversion and may maintain the topological surface state while the bulk changes to semimetal, and at phase III, the band gap closes, making the system fully bulk metallic.

ACKNOWLEDGMENTS

We thank colleagues F. H. Li, H. Yan, and B. Jones at Stanford University and beamline scientists S. T. C. Park, S. Sinogeikin, Y. Meng (APS), J. Yan, B. Chen, and A. MacDowell (ALS) for their assistance and thank W. Jing and Y. He for meaningful discussions. We also thank the reviewers for their constructive comments. Z.Z. is supported through the Stanford Institute for Materials and Energy Sciences, supported by the U.S. Department of Energy, Materials Sciences and Engineering Division, under Award No. DE-AC02-76SF00515. S.W. is supported by EFree, an Energy Frontier Research Center funded by the US Department of Energy, Office of Science, Office of Basic Energy Sciences, under Award No. DE-SG0001057. H.Z. is supported by the Army Research Office Award No. W911NF-09-1-0508.

[1]X.-L. Qi and S.-C. Zhang, Rev. Mod. Phys. **83**, 1057 (2011).
[2]J. E. Moore, Nature **464**, 194 (2010).
[3]X.-L. Qi and S.-C. Zhang, Phys. Today **63**(1), 33 (2010).
[4]M. Z. Hasan and C. L. Kane, Rev. Mod. Phys. **82**, 3045 (2010).
[5]H. Zhang, C.-X. Liu, X.-L. Qi, X. Dai, Z. Fang, and S.-C. Zhang, Nat. Phys. **5**, 438 (2009).
[6]Y. L. Chen, J. G. Analytis, J.-H. Chu, Z. K. Liu, S.-K. Mo, X. L. Qi, H. J. Zhang, D. H. Lu, X. Dai, Z. Fang, S. C. Zhang, I. R. Fisher, Z. Hussain, and Z.-X. Shen, Science **325**, 178 (2009).
[7]Y. Xia, D. Qian, D. Hsieh, L. Wray, A. Pal, H. Lin, A. Bansil, D. Grauer, Y. S. Hor, R. J. Cava, and M. Z. Hasan, Nat. Phys. **5**, 398 (2009).
[8]W. Zhang, R. Yu, H.-J. Zhang, X. Dai, and Z. Fang, New J. Phys. **12**, 065013 (2010).
[9]D. Hsieh, Y. Xia, D. Qian, L. Wray, F. Meier, J. H. Dil, J. Osterwalder, L. Patthey, A. V. Fedorov, H. Lin, A. Bansil, D. Grauer, Y. S. Hor, R. J. Cava, and M. Z. Hasan, Phys. Rev. Lett. **103**, 146401 (2009).

[10]W. Zhang, R. Yu, W. Feng, Y. Yao, H. Weng, X. Dai, and Z. Fang, Phys. Rev. Lett. **106**, 156808 (2011).
[11]S. Lee, J. In, Y. Yoo, Y. Jo, Y. C. Park, H.-J. Kim, H. C. Koo, J. Kim, B. Kim, and K. L. Wang, Nano Lett. **12**, 4194 (2012).
[12]A. Sulaev, P. Ren, B. Xia, Q. H. Lin, T. Yu, C. Qiu, S.-Y. Zhang, M.-Y. Han, Z. P. Li, W. G. Zhu, Q. Wu, Y. P. Feng, L. Shen, S.-Q. Shen, and L. Wang, AIP Adv. **3**, 032123 (2013).
[13]H. Peng, K. Lai, D. Kong, S. Meister, Y. Chen, X.-L. Qi, S.-C. Zhang, Z.-X. Shen, and Y. Cui, Nat. Mater. **9**, 225 (2010).
[14]F. Xiu, L. He, Y. Wang, L. Cheng, L.-T. Chang, M. Lang, G. Huang, X. Kou, Y. Zhou, X. Jiang, Z. Chen, J. Zou, A. Shailos, and K. L. Wang, Nat. Nanotech. **6**, 216 (2011).
[15]V. E. Sacksteder, S. Kettemann, Q. S. Wu, X. Dai, and Z. Fang, Phys. Rev. B **85**, 205303 (2012).
[16]F. Virot, R. Hayn, M. Richter, and J. van den Brink, Phys. Rev. Lett. **106**, 236806 (2011).
[17]R. Xu, A. Husmann, T. F. Rosenbaum, J. E. Enderby, and P. B. Littlewood, Nature (London) **390**, 57 (1997).
[18]A. Husmann, J. B. Betts, G. S. Boebinger, A. Migliori, T. F. Rosenbaum, and M.-L. Saboungi, Nature (London) **417**, 421 (2002).
[19]M. M. Parish and P. B. Littlewood, Nature (London) **426**, 162 (2003).
[20]J. Hu, T. F. Rosenbaum, and J. B. Betts, Phys. Rev. Lett. **95**, 186603 (2005).
[21]J. Hu, M. M. Parish, and T. F. Rosenbaum, Phys. Rev. B **75**, 214203 (2007).
[22]A. A. Abrikosov, Phys. Rev. B **58**, 2788 (1998).
[23]A. A. Abrikosov, Phys. Rev. B **60**, 4231 (1999).
[24]M. Lee, T. F. Rosenbaum, M.-L. Saboungi, and H. S. Schnyders, Phys. Rev. Lett. **88**, 066602 (2002).
[25]M. D. Banus and M. C. Finn, J. EIectrochem. Soc. **116**, 91 (1969).
[26]A. van der Lee and J. L. de Boer, Acta Cryst. C **49**, 1444 (1993).
[27]S. Miyatani, J. Phys. Soc. Jpn. **13**, 341 (1958).
[28]C. R. Veale, J. Less-Common Met. **11**, 50 (1966).
[29]See Supplemental Material at http://link.aps.org/supplemental/10.1103/PhysRevB.88.024120 for sample characterization, Rietveld refinement results, and crystallographical information.
[30]JADE, Computer Code for XRD Pattern Processing (Materials Data, Inc., Livermore, CA, 2005).
[31]B. H. Toby, J. Appl. Cryst. **34**, 210 (2001).
[32]G. Kresse and D. Joubert, Phys. Rev. B **59**, 1758 (1999).
[33]G. Kresse and J. Hafner, Phys. Rev. B **47**, 558 (1993).
[34]J. P. Perdew, K. Burke, and M. Ernzerhof, Phys. Rev. Lett. **77**, 3865 (1996).
[35]P. Hohenberg and W. Kohn, Phys. Rev. **155**, 864 (1964).
[36]P. E. Blöchl, Phys. Rev. B **50**, 17953 (1994).
[37]A. Polian, M. Gauthier, S. M. Souza, D. M. Trichês, J. Cardosode-Lima, and T. A. Grandi, Phys. Rev. B **83**, 113106 (2011).
[38]R. Vilaplana, D. Santamaría-Pérez, O. Gomis, F. J. Manjón, J. González, A. Segura, A. Muñoz, P. Rodríguez-Hernández, E. Pérez-González, V. Marín-Borrás, V. Muñoz-Sanjose, C. Drasar, and V. Kucek, Phys. Rev. B **84**, 184110 (2011).
[39]J. R. Ziman, *Principles of the Theory of Solids* (Cambridge University Press, Cambridge, UK, 1972), pp. 250–254.